6932 *Biochemistry* **2009,** *48,* 6932–6939
DOI: 10.1021/bi900713j

BIOCHEMISTRY
including biophysical chemistry & molecular biology
Article

Hydrogen Bond Coupling in the Ketosteroid Isomerase Active Site[†,‡]

Paul A. Sigala,[§] Jose M. M. Caaveiro,[∥,⊥] Dagmar Ringe,[∥] Gregory A. Petsko,[∥] and Daniel Herschlag*[,§]

[§]*Department of Biochemistry, Stanford University, Stanford, California 94305, and* [∥]*Departments of Biochemistry and Chemistry and Rosenstiel Basic Medical Sciences Research Center, Brandeis University, Waltham, Massachusetts 02454* [⊥]*Present address: Laboratory of Physical Biochemistry, Graduate School of Frontier Sciences, University of Tokyo, Tokyo, Japan*

Received April 25, 2009; Revised Manuscript Received May 26, 2009

ABSTRACT: Hydrogen bond networks are key elements of biological structure and function. Nevertheless, their structural properties are challenging to assess within complex macromolecules. Hydrogen-bonded protons are not observed in the vast majority of protein X-ray structures, and static crystallographic models provide limited information regarding the dynamical coupling within hydrogen bond networks. We have brought together 1.1−1.3 Å resolution X-ray crystallography, ^{1}H NMR, site-directed mutagenesis, and deuterium isotope effects on the geometry and chemical shifts of hydrogen-bonded protons to probe the conformational coupling of hydrogen bonds donated by Y16 and D103 in the oxyanion hole of bacterial ketosteroid isomerase. Our results suggest a robust physical coupling of the equilibrium structures of these two hydrogen bonds such that a lengthening of one hydrogen bond by as little as 0.01 Å results in a shortening of the neighbor by a similar magnitude. Furthermore, the structural rearrangements detected by NMR in response to mutations within the active site hydrogen bond network can be explained on the basis of the observed coupling. The results herein elucidate fundamental structural properties of hydrogen bonds within the idiosyncratic environment of an enzyme active site and provide a foundation for future experimental and computational explorations of the role of coupled motions within hydrogen bond networks.

Hydrogen bonds are central to the structure and function of biological macromolecules. Despite the ubiquitous presence of hydrogen bonds in biology and their extensive study in small molecules (*1*, *2*), incisive dissection of hydrogen bond properties within proteins and other large biomolecules remains challenging. Indeed, electron density for hydrogen-bonded protons is not typically observed in high-resolution X-ray diffraction studies of proteins. Thus, hydrogen bond formation must be indirectly assessed from the proximity of putative donor and acceptor heavy nuclei observed crystallographically. Furthermore, static structural models provide limited insight regarding the structural plasticity and conformational dynamics of hydrogen bonds, whose distances can vary by up to ∼1 Å based on the specific properties of the donor and acceptor groups and the local structural environment (*1*, *3*−*6*).

Networks of adjoining hydrogen bonds commonly form in proteins, where they span secondary structures, link disparate domains, connect active site residues, position bound ligands, and stabilize charge rearrangement in reacting substrates (*7*). Recent studies suggest that the unique structural and dynamical properties of hydrogen bond networks play important roles in coupling the motions of distal groups for allostery and signal propagation (*6*, *8*−*10*) and in fine-tuning the positions of protein and ligand groups, especially those involved in proton-coupled electron transfer (*11*−*13*). While our understanding of the dynamic motions with protein structural elements spanning a broad range of distance and time scales is rapidly improving (*14*−*18*), direct assessment of the physical coupling between groups remains challenging (*19*, *20*).

Bacterial ketosteroid isomerase (KSI)[1] from *Pseudomonas putida* (pKSI) and *Commamonas testosteroni* (tKSI) has provided a powerful experimental system for dissecting the physical properties of key active site hydrogen bonds. KSI catalyzes the isomerization of steroid substrates via formation of a dienolate intermediate (Scheme 1A) (*21*). Localized negative charge on the oxygen of the reaction intermediate is stabilized by hydrogen bonds donated by Y16 (pKSI numbering) and protonated D103 (*22*, *23*), which form a conserved hydrogen bond network within an active site oxyanion hole via the additional hydrogen bond donated by Y57 to the hydroxyl of Y16 (*24*). The substantial rate decreases observed upon mutation of Y16 (*25*, *26*)

[†]This work was funded by an NSF grant to D.H., D.R., and G.A.P. (MCB-0641393). P.A.S. was supported in part by HHMI and Gerald Lieberman Predoctoral Fellowships. Portions of this research were conducted at the Stanford Synchrotron Radiation Laboratory, which is supported by the Department of Energy and the National Institutes of Health.

[‡]Coordinates for the pKSI$^{D103N/D40N}$·equilenin crystal structure have been deposited in the RCSB Protein Data Bank as entry 3FZW.

*To whom correspondence should be addressed: E-mail: herschla@stanford.edu. Phone: (650) 723-9442. Fax: (650) 723-6783.

[1]Abbreviations: KSI, ketosteroid isomerase; pKSI, KSI from *Pseudomonas putida*; tKSI, KSI from *Commamonas testosteroni*; PDB, Protein Data Bank.

 Published on Web 05/26/2009

Scheme 1: (A) Mechanism of KSI-Catalyzed Steroid Isomerization and (B) Schematic Depiction of the Reaction Intermediate Analogue, Equilenin, Bound at the KSI Active Site

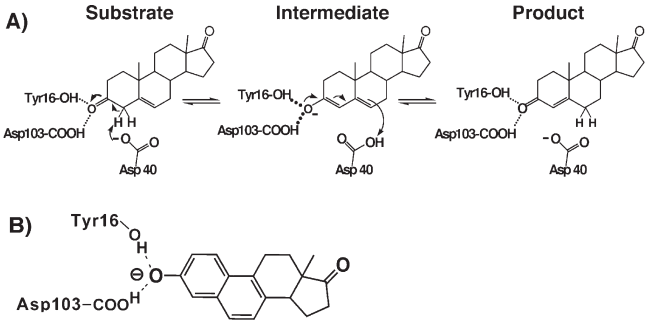

and D103 (*23*, *27*, *28*) and results from linear free energy relationship studies of KSI (*4*, *29*) suggest important functional roles for these hydrogen bonds.

The steroid, equilenin, and single-ring phenolates bind in the KSI active site, accept 2.5−2.6 Å hydrogen bonds from Y16 and D103 (*22*, *29*, *30*), and serve as analogues of the dienolate reaction intermediate (Scheme 1B). The hydrogen-bonded protons donated by Y16 and D103 to the oxygen of KSI-bound phenolates appear as far-downfield peaks (14−18 ppm) in ^{1}H NMR spectra, providing a spectroscopic probe with which to dissect hydrogen bond properties. We previously showed that increasing oxyanion charge localization, analogous to the charge rearrangement during steroid isomerization, results in a shortening of these hydrogen bonds by ~0.02 Å per unit increase in oxyanion pK_a (*29*). The introduction of structural constraints within the oxyanion hole, however, can prevent such hydrogen bond shortening, highlighting the ability of binding interactions within enzyme active sites to alter hydrogen bond properties from those in solution (*4*).

Herein we use X-ray crystallography, site-directed mutagenesis, NMR, and hydrogen−deuterium geometric isotope effects to address two critical questions regarding the physical coupling of Y16 and D103. First, are the Y16 and D103 hydrogen bonds conformationally coupled, such that a structural perturbation to one is propagated to the other? And second, what is the distance scale of the observed coupling? Our results suggest a robust physical coupling of the equilibrium structures of the Y16 and D103 hydrogen bonds, with a lengthening of one by as little as 0.01 Å resulting in a shortening of the neighboring hydrogen bond by a similar magnitude.

MATERIALS AND METHODS

Materials. All reagents were of the highest purity commercially available. 3-F-5-CF_3-phenol, 3,4,5-F_3-phenol, and equilenin were purchased from Oakwood Products, Matrix Scientific, and Steraloids, respectively. DMSO-d_6 and D_2O were purchased from Cambridge Isotopes. All buffers were prepared with reagent-grade chemicals or better.

KSI Mutagenesis, Expression, and Purification. QuikChange site-directed mutagenesis was used to introduce the D40N, D103N, and Y57F mutations, which were confirmed by sequencing miniprep DNA from DH5α cells on an ABI3100 capillary sequencer. KSI was expressed and purified as previously described (*29*). The final purity was >99%, as estimated from a Coomassie-stained SDS−PAGE gel. Protein concentrations were determined using the calculated molar extinction coefficient in 6 M guanidine chloride (*31*).

Absorbance Spectra of KSI·Phenolate Complexes. To confirm that phenols bind as ionized phenolates to KSI containing the D103N or Y57F mutation, absorbance spectra of 3,4,-5-F_3-phenol were acquired in a microcuvette with a Uvikon 9310 absorbance spectrophotometer. Spectra of 50 μM 3,4,5-F_3-phenol in 10 mM HCl (pH 2) and 10 mM NaOH (pH 12) were compared with the spectrum of phenol at the same concentration in 40 mM potassium phosphate (KP_i) buffer (pH 7.2) in the presence of 300 μM $tKSI^{D103N/D40N}$ or $tKSI^{Y57F/D40N}$ (phenol >95% bound, data not shown), after subtraction of the free enzyme spectrum. Spectra for both mutants indicated binding as the ionized phenolate.

KSI X-ray Crystallography. $pKSI^{D103N/D40N}$·equilenin cocrystals in space group *C*2 were obtained using the hanging drop vapor diffusion method by mixing 2 μL of $pKSI^{D103N/D40N}$ at 25 mg/mL preincubated with equilenin (KSI:equilenin molar ratio of 1:1.2) and 2 μL of reservoir solution [1.4 M ammonium sulfate and 6.5% (v/v) 2-propanol (pH 7.0)]. Rod-shaped crystals appeared after incubation for 1 week at room temperature. Cryoprotection was achieved by soaking the crystals in a solution of mother liquor containing 20% glycerol. Crystals were shock-cooled by immersion into liquid nitrogen. Diffraction data from single crystals maintained at 100 K were collected at beamline BL9-1 of the Stanford Synchrotron Radiation Laboratory (Stanford Linear Accelerator Center, Stanford, CA). Data were integrated and scaled using the HKL2000 program package. An initial model of the protein was obtained by the molecular replacement method with PHASER (*32*), using the coordinates of a previously reported structure of $pKSI^{D40N}$ (PDB entry 2PZV). Refinement and manual rebuilding were conducted using REFMAC5 (*33*) and COOT (*34*), respectively. Model quality was assessed using PROCHECK (*35*), and the Ramachandran plot showed no residues outside the allowed regions. Coordinate uncertainty was estimated using the diffraction-component precision index (DPI) developed by Cruickshank (*36*) and carried out in REFMAC5. Structural coordinates have been deposited in the RCSB Protein Data Bank as entry 3FZW.

KSI NMR Spectroscopy. ^{1}H NMR spectra of KSI were acquired at the Stanford Magnetic Resonance Laboratory on an 800 MHz Varian ^{UNITY}INOVA spectrometer running VNMR version 6.1C and equipped with a 5 mm, triple-resonance, gradient ^{1}H(^{13}C/^{15}N) probe. NMR samples consisted of 0.5 mM $tKSI^{D40N}$ and 0.5−5.0 mM substituted phenol in 40 mM KP_i buffer (pH 7.2), 1 mM EDTA, and 10% (v/v) DMSO-d_6 (which served as the lock solvent and prevented freezing at sub-zero temperatures) in 5 mM Shigemi symmetrical microtubes at −3.0 ± 0.5 °C. One-dimensional proton spectra were acquired using the 1331 binomial pulse sequence (*37*) to suppress the water signal, with a spectral width of 30 ppm (carrier frequency set on the water resonance) and an excitation maximum of 14−18 ppm. Data were collected for 512−5120 scans and processed using a 10 Hz line broadening and baseline correction applied over the peaks of interest. Chemical shifts were referenced internally to the water resonance (5.1 at −3.0 °C) and externally to a sample of sodium 3-trimethylsilylpropionate-2,2,3,3-d_4 (0 ppm) under the same buffer conditions (*38*). Hydrogen bond O···O and H···O distances were estimated from the observed chemical shifts for the detected hydrogen-bonded protons using the correlation functions given in refs (*39*) and (*40*), respectively.

RESULTS AND DISCUSSION

To assess the presence of physical coupling between the Y16 and D103 hydrogen bonds in the KSI oxyanion hole, we first took a mutagenesis approach. We hypothesized that a structural perturbation introduced at either the D103 or Y16 hydrogen bond via mutation might be accompanied by a structural rearrangement in the adjoining hydrogen bond neighbor if these interactions were indeed physically coupled via hydrogen bond formation to the common oxyanion acceptor. If no rearrangement in the adjoining, unmodified hydrogen bond neighbor were detected, then direct physical coupling of these hydrogen bonds might either be absent or be overwhelmed by larger-scale individual or collective motions of groups within the KSI active site.

The mutations chosen to site-specifically perturb either the D103 or Y16 hydrogen bond formed to the oxyanion of equilenin or phenolates were D103N and Y57F, which have minor effects on active site structure and result in small (3−30-fold) reductions in KSI activity (k_{cat}). These mutants (in the D40N background)[2] bind ionized phenolates and maintain two hydrogen bonds to the phenolate or equilenin oxyanion (Figure S1 of the Supporting Information). We expected the N···O hydrogen bond in the D103N mutant to be lengthened relative to unmodified D103 on the basis of the higher pK_a of an Asn side chain amide (∼17) (*41*) relative to the hydroxyl of D103 (∼8) (*27*) and hence greater pK_a mismatch with the bound oxyanion (*5*, *29*). We similarly expected the Y57F mutation, which ablates a hydrogen bond to Y16 and presumably weakens its ability to donate a hydrogen bond, to result in a lengthening of the Y16·oxyanion hydrogen bond.

We first determined a high-resolution X-ray structure of the pKSI$^{D103N/D40N}$·equilenin complex to directly assess the structural consequences of the D103N mutation and any propagated effects on the Y16·equilenin O···O distance relative to the previously published 1.1 Å resolution pKSI·equilenin structure (PDB entry 1OH0). We then exploited the exquisite sensitivity of NMR and the ability to spectroscopically observe the hydrogen-bonded protons of Y16 and D103 to test for propagated effects from the D103N and Y57F mutations that would signal the presence of physical coupling within the oxyanion hole hydrogen bond network. Finally, we applied an isotopic substitution method to directly probe conformational coupling in the unmodified hydrogen bond network of tKSI^{D40N} in the absence of the potential indirect effects from oxyanion hole mutations.

Structure of the pKSI$^{D103N/D40N}$·Equilenin Complex at 1.3 Å Resolution. A previously published 1.1 Å resolution X-ray structure of the pKSI·equilenin complex (*22*) identified short average O···O distances of 2.51 and 2.56 Å for the hydrogen bonds donated by D103 and Y16, respectively, to the oxyanion of bound equilenin (Table 1). To assess the effect of the D103N mutation on these hydrogen bond distances, we determined the X-ray structure of the pKSI$^{D103N/D40N}$·equilenin complex. Data collection and refinement statistics are listed in Table 2. The overall KSI structure obtained at 1.3 Å resolution is nearly identical to that observed previously for the pKSI·equilenin complex, with a root-mean-square deviation between the two structures of 0.3 Å for backbone atoms. The electron density map of the pKSI$^{D103N/D40N}$·equilenin structure, contoured in Figure 1A at 1.5σ, shows well-defined density for the modeled atomic positions within the active site, with no indication of alternative ligand or side chain conformations. We observed electron density for an ordered water molecule in the oxyanion hole within hydrogen bonding distance (3.27 Å) of the equilenin oxyanion (Figure S2 of the Supporting Information). This water was not reported in the pKSI·equilenin structure (PDB entry 1OH0).

The refined orientation of bound equilenin is very similar to that observed previously for the pKSI·equilenin complex, with equilenin positioned in both active sites to accept hydrogen bonds from Y16 and D103 or N103 (Figure 1B). Subtle displacements in the positions of the equilenin oxyanion and the N103 side chain in the pKSI$^{D103N/D40N}$·equilenin complex, however, result in a lengthened average N···O distance of 2.89 Å relative to the 2.51 Å O···O distance observed for D103 in the pKSI·equilenin complex (Table 1). This length difference of 0.38 Å is clearly distinguishable at the stated resolutions and 0.03−0.05 Å estimated coordinate error for the two structures (see Table 1 and Materials and Methods).

Is lengthening of the hydrogen bond donated by residue 103 to the equilenin oxyanion accompanied by a change in the length of

Table 1: Refined Hydrogen Bond O···O Distances to Equilenin in the KSI Oxyanion Hole

structure (PDB entry)[a]	resolution (Å)[b]	Tyr16−equilenin (Å)	Asp/Asn103−equilenin (Å)
pKSI·equilenin (1OH0)	1.1	2.55	2.54
		2.56	2.48
pKSI$^{D103N/D40N}$·equilenin (3FZW)	1.3	2.50	2.90
		2.52	2.88

[a] The asymmetric unit of both structures contained two independently refined monomers. [b] Coordinate errors are estimated to be 0.03 Å (1OH0) and 0.05 Å (3FZW) on the basis of ref (*36*).

Table 2: Crystallographic Data and Refinement Statistics for the pKSI$^{D103N/D40N}$·Equilenin Complex

resolution range (Å)	55.05−1.32
space group	*C*2
a (Å)	86.9
b (Å)	71.2
c (Å)	50.5
α (deg)	90.0
β (deg)	89.9
γ (deg)	90.0
no. of unique reflections	68149
completeness (%)	94.0
multiplicity	2.9
R_{merge} (%)[a]	8.8
$I/\sigma_{overall}$ ($I/\sigma_{high\ res}$)	10.3 (2.4)
Refinement Statistics	
no. of residues	250
no. of waters	239
R_{work} (%)[b]	14.9
R_{free} (%)[c]	18.3
rmsd for bonds (Å)	0.023
rmsd for angles (deg)	2.1

[a] $R_{merge} = \sum_{hkl}\sum|I(hkl)_i - [I(hkl)]|/\sum_{hkl}\sum_i I(hkl)_i$. [b] $R_{work} = \sum_{hkl}|F(hkl)_o - [F(hkl)_c]|/\sum_{hkl}F(hkl)_o$. [c] R_{free} was calculated exactly as R_{work}, where $F(hkl)_o$ values were taken from 5% of the data not included in refinement.

[2]The D40N mutation mimics the protonated general base, D40, present in the KSI−intermediate complex.

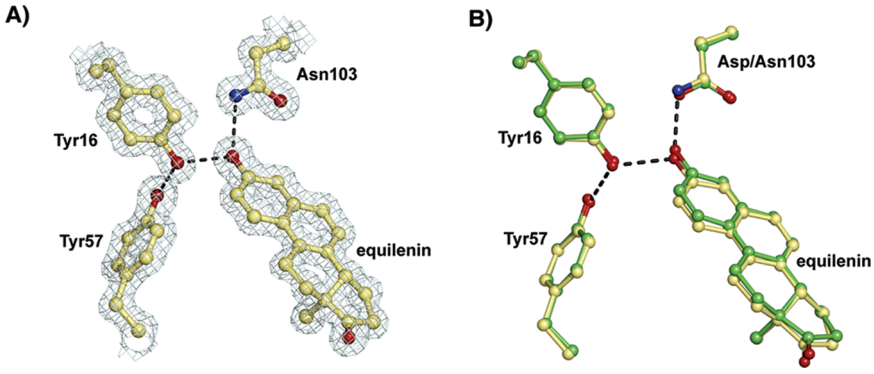

FIGURE 1: Crystal structure of equilenin bound at the active site of pKSI$^{D103N/D40N}$. (A) Sigma-A-weighted $2F_o - F_c$ electron density map (contoured at 1.5σ) showing equilenin bound in the KSI oxyanion hole, positioned to receive hydrogen bonds from Tyr16 and Asn103. (B) Superposition of the 1.3 Å resolution pKSI$^{D103N/D40N}$·equilenin (carbon atoms colored yellow) and 1.1 Å resolution pKSI·equilenin (PDB entry 1OH0, carbon atoms colored green) structures.

the Y16·equilenin hydrogen bond, as expected for physically coupled interactions? The average observed O···O distance for the Y16·equilenin hydrogen bond in the pKSI$^{D103N/D40N}$·equilenin structure is 2.51 Å, which is 0.05 Å shorter than the corresponding distance observed for the KSI·equilenin complex (Table 1). This apparent shortening is consistent with a modest coupling of these hydrogen bonds. However, the observed 0.05 Å change is similar to the 0.03−0.05 Å estimated coordinate uncertainty of the two structures, rendering a definitive conclusion about the scale of coupling problematic. Furthermore, the small change in O···O distance may mask a larger change in the position of the hydrogen-bonded proton of Y16. As stated above, hydrogen-bonded protons are not typically observed in high-resolution X-ray structures, even structures obtained at nearly 1.0 Å resolution. To overcome this limitation, we next turned to ^{1}H NMR to directly detect the hydrogen-bonded protons in the oxyanion hole and assess changes in their positions in response to the D103N and Y57F mutations.

NMR Assessment of Oxyanion Hole Hydrogen Bond Coupling via the D103N and Y57F Mutations. Extensive studies of O−H···O hydrogen bonds in small molecule complexes by neutron diffraction and solid state NMR have established a strong correlation between the observed chemical shift of a hydrogen-bonded proton and the O···O and H···O hydrogen bond distances (*39*, *40*). Thus, changes in the observed chemical shifts of hydrogen-bonded protons can be used to estimate changes in the O···O and H···O hydrogen bond distances (*42*), as previously reported for KSI·phenolate complexes (*4*, *29*).

To assess whether structural perturbations to the D103 and Y16 hydrogen bonds due to the D103N and Y57F mutations, respectively, result in propagated rearrangements within the adjoining, unmodified hydrogen bond, we acquired NMR spectra of 3,4-dinitrophenolate bound to tKSI^{D40N}, tKSI$^{D103N/D40N}$, and tKSI$^{Y57F/D40N}$. As shown in Figure 2, two far-downfield peaks at 14.0 and 14.2 ppm are observed for the tKSI^{D40N}·3,4-dinitrophenolate complex. These peaks have previously been assigned to the hydrogen-bonded protons donated by D103 and Y16 to the phenolate oxygen, based on H−H NOESY spectra and oxyanion hole mutations (*29*). These experiments, however, cannot distinguish which of the two peaks arises from Y16 and which is from D103; the conclusions herein do not require further assignment of these peaks.

Lengthening of the D103 hydrogen bond via the D103N mutation resulted in an ~1 ppm downfield shift in the NMR

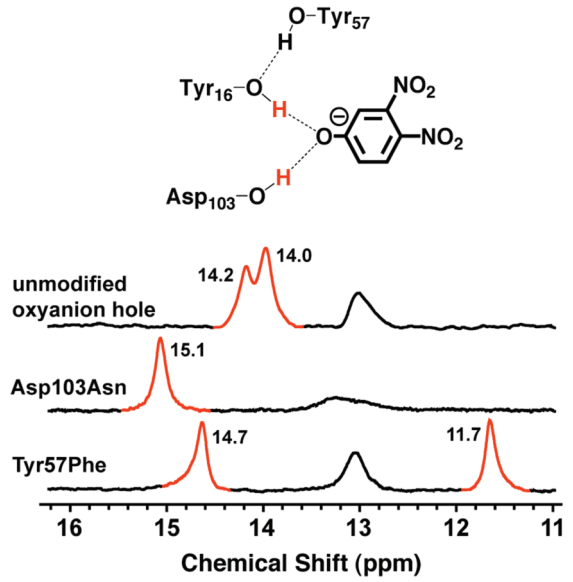

FIGURE 2: Downfield region of ^{1}H NMR spectra of KSI hydrogen bond mutants bound to 3,4-dinitrophenolate. Downfield NMR peaks corresponding to oxyanion hole hydrogen-bonded protons are colored red. All proteins carried the D40N mutation, as explained in the text. The spectrum of the tKSI^{D40N}·3,4-dinitrophenolate complex was previously published (*29*).

peak position corresponding to the remaining, unmutated hydrogen-bonded proton of Y16 (Figure 2; see further description of the peak assignments in the mutant spectra in the Supporting Information). This chemical shift change is consistent with a ~0.05 contraction in the O···O and H···O hydrogen bond distances, based on the correlation functions given in refs (*39*) and (*40*), and very similar to the 0.05 Å shortening observed in the pKSI$^{D103N/D40N}$·equilenin X-ray structure described above. The Y57F mutation maintains two O−H···O hydrogen bonds to the bound oxyanion but is expected to lengthen the Y16 hydrogen bond (see above). This mutation resulted in one peak moving ~2.4 ppm upfield and the other moving ~0.6 ppm downfield relative to the tKSI^{D40N}·3,4-dinitrophenolate complex (Figure 2). These chemical shift changes are expected for a 0.13 Å lengthening of the Y16 hydrogen bond and a concomitant 0.03 Å shortening of the D103 hydrogen bond. For hydrogen bonds donated to the same acceptor, the shortening of one in response to lengthening of the other has previously been termed "anticooperative", based on studies of small molecules (*43*, *44*).

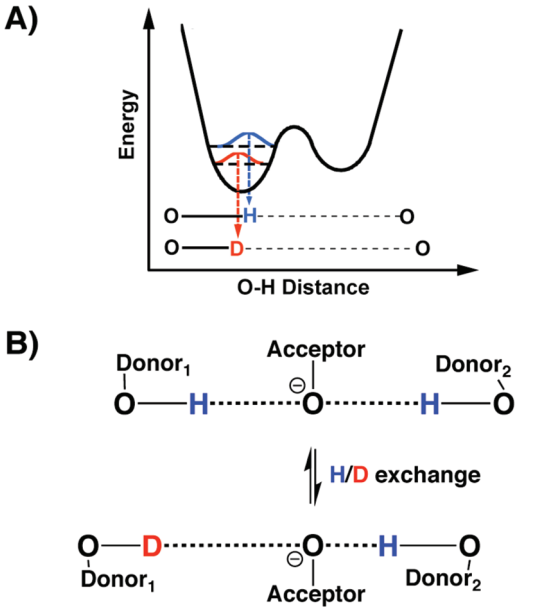

FIGURE 3: Schematic depictions of hydrogen bond changes upon deuterium substitution. (A) For short hydrogen bonds with a shallow barrier to proton transfer, anharmonicity in the shape of the hydrogen bond potential energy well and the lower zero-point energy for deuterium result in an O−D bond shorter than the original O−H bond by 0.01−0.02 Å and a lengthening of the O···O distance by a similar magnitude (*2*, *45*, *47*). This figure is for illustrative purposes only and is not meant to convey the shape of the potential energy well for KSI oxyanion hole hydrogen bonds. (B) Conformational changes within a hydrogen bond network upon isotopic substitution. Lengthening of a hydrogen bond upon deuterium substitution leads to shortening of a neighboring hydrogen bond to the same acceptor.

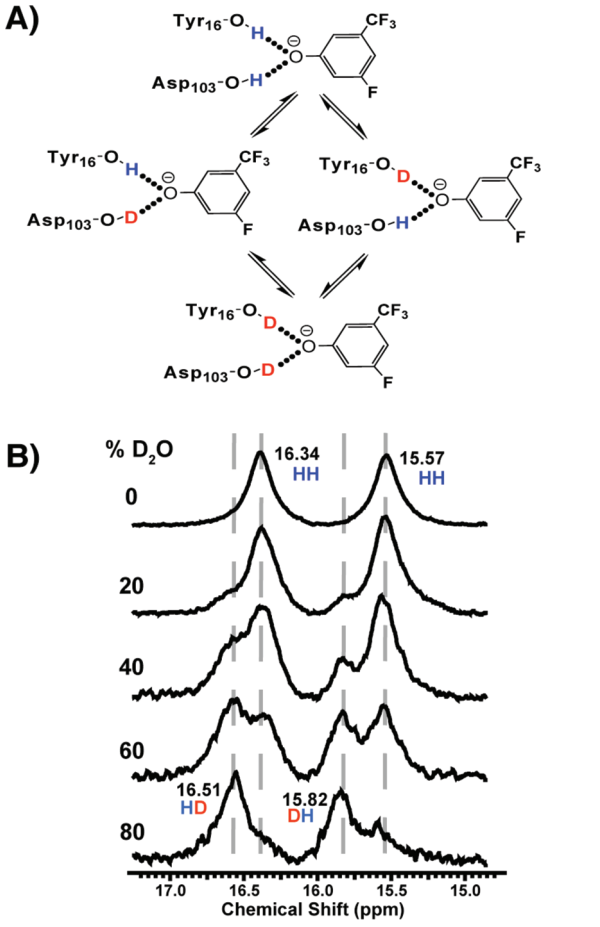

FIGURE 4: NMR detection of conformational coupling between the hydrogen bonds donated by Tyr16 and Asp103 in the KSI oxyanion hole. (A) Hydrogen−deuterium isotopologues of hydrogen bonds in the KSI oxyanion hole. (B) ^{1}H NMR spectra of tKSI^{D40N}·3-F-5-CF_3-phenolate complexes in solutions containing increasing amounts of D_2O. The spectrum in 0% D_2O was previously published (*29*).

These changes suggest a modest scale of conformational coupling between the hydrogen bonds within the KSI oxyanion hole, such that a structural perturbation to one is propagated to its connected hydrogen bond neighbors. Nevertheless, structural rearrangements within nearby groups that are in van der Waals contact with Y16, D103, and the bound phenolate, in response to these mutations, could be the source of the observed spectral shifts rather than direct propagation of conformational changes through the hydrogen bond network. The presence of an ordered water molecule in mutant oxyanion holes (observed in the pKSI$^{D103N/D40N}$·equilenin structure described above) that is not observed in the pKSI·equilenin structure containing the unmodified oxyanion hole may further complicate the comparison of hydrogen bond properties between the mutant and wild-type oxyanion holes. We therefore applied an isotopic substitution method to directly probe hydrogen bond coupling within the intact hydrogen bond network in the KSI oxyanion hole with minimal secondary perturbation.

Direct Detection of Physical Coupling between the Y16 and D103 Hydrogen Bonds. Extensive structural studies of hydrogen bonds in small molecules have revealed that short hydrogen bonds with O···O distances of less than ~2.7 Å are subtly lengthened upon substitution of the bridging hydrogen with deuterium or tritium (*1*, *2*, *45*, *46*). These changes have been ascribed to anharmonicity in the shape of the hydrogen bond potential energy well that arises from a shallow barrier for proton transfer. In such cases, the lower zero-point energy for deuterium results in a shorter O−D bond than the original O−H bond by 0.01−0.02 Å and an increase in the O···O distance by a similar magnitude (*2*, *47*). These changes are shown schematically in Figure 3A. Subtle changes in hydrogen bond length upon isotopic substitution can be detected by NMR and have been reported for small molecules in aprotic organic solvents (*2*, *47*, *48*), in ubiquitin (*49*), and in the active site of chymotrypsin (*50*).

For two short small-molecule hydrogen bonds donated to a common acceptor, deuterium substitution of one hydrogen bond has been observed to result in an increased chemical shift of the proton bridging the neighboring, unsubstituted hydrogen bond. This scenario is shown schematically in Figure 3B (*43*, *51*, *52*). These observations are consistent with a lengthening of the first hydrogen bond upon deuterium substitution (due to a shorter O−D σ bond) and a shortening of the adjoining, unmodified hydrogen bond (due to an increase in the O−H bond length which leads to an increased proton chemical shift). The propagation of such geometric perturbations through hydrogen bond networks as a consequence of deuterium substitution provides direct evidence for the robust physical coupling of the equilibrium conformations of adjoining hydrogen bonds. This coupling may derive from an increase in negative charge localization on the acceptor oxygen that occurs upon lengthening of one hydrogen bond from deuterium substitution such that the proton bridging the neighboring hydrogen bond moves toward the acceptor oxygen and the H···O−acceptor distance decreases (Figure 3B). Transmission of geometric isotope effects within hydrogen bond networks in proteins has previously been shown for cytosine deaminase (*53*) and photoactive yellow protein (*6*).

We applied a similar deuterium substitution strategy to directly probe physical coupling between the Y16 and D103 hydrogen bonds in the unmodified KSI oxyanion hole, as follows. As the D_2O content of a KSI solution increases, the hydrogen-bonded protons in the oxyanion hole exchange with deuterium to populate four possible isotopologues, shown in Figure 4A. Although exchange of a hydrogen-bonded proton for a deuteron renders that hydrogen bond undetectable by ^1H NMR, its adjoining hydrogen-bonded neighbor remains detectable if its bridging proton has not exchanged with solvent deuterons. This is the case for the central HD and DH isotopologues shown in Figure 4A. Given the short 2.5−2.6 Å hydrogen bond O···O distances previously reported for KSI^{D40N}-bound phenolates (*29*), we expected deuterium substitution of either hydrogen bond to lengthen it by 0.01−0.02 Å based on the geometric perturbations reported for similar-length hydrogen bonds in small molecules (*45*). If the structures of the Y16 and D103 hydrogen bonds were indeed physically coupled, as suggested by the mutagenesis results presented earlier, then deuteration of one hydrogen bond would be expected to result in a shortening of the adjoining hydrogen bond neighbor and more downfield chemical shift for its bridging proton. Thus, in the case of coupling, we expected to observe a second, more downfield resonance for each of the Y16 and D103 hydrogen-bonded proton peaks (four peaks total) in solutions with an increasing level of D_2O, with the new peaks corresponding to the HD isotopologues in Figure 4A. Alternatively, if the Y16 and D103 hydrogen bonds were not strongly coupled, then we would expect to observe only two peaks that decreased in intensity with an increase in D_2O content.

In the absence of solvent D_2O, two peaks are observed for the $tKSI^{D40N}$·3-F-5-CF_3-phenolate complex (Figure 4B), as expected for the exclusive presence of the HH isotopologue. With an increase in D_2O content and population of the HD hydrogen bond isotopologues, a second, more-downfield peak is indeed observed for each peak. The intensity of the new HD peaks increases relative to the HH peaks with an increase in D_2O content, as the isotopologue equilibrium shifts in favor of the HD species. The observation of four peaks indicates that the chemical shift and hence the length of the D103 or Y16 hydrogen bond are altered upon structural perturbation of the neighboring hydrogen bond via deuterium substitution. This result provides direct evidence that the equilibrium structures of the oxyanion hole hydrogen bonds are physically coupled.

For both downfield peaks, the new resonance that appears with an increase in D_2O content is shifted ~0.2 ppm downfield relative to the HH isotopologue peak (Figure 4B). This 0.2 ppm shift is expected for shortening of the D103 and Y16 hydrogen bond H···O and O···O distances by ~0.01 Å. This estimated 0.01 Å shortening detected in the hydrogen bond whose proton has not exchanged is on the same scale as the ~0.01 Å lengthening expected in the hydrogen bond neighbor that has been deuterated (Figure 4A). The similar scale of the primary and propagated distance perturbations provides evidence for a robust degree of coupling of the Y16 and D103 hydrogen bond structures. This coupling is very similar to that observed in the structurally similar oxyanion hole of photoactive yellow protein (*6*).

While the observed geometric isotope effects provide evidence for robust coupling of hydrogen bond conformations on the ~0.01 Å scale (i.e., the primary and propagated distance changes are both ~0.01 Å), the smaller propagated effects observed upon mutation suggest that coupling on a larger scale may be attenuated by structural constraints and rearrangements within the active site. Indeed, the 0.4 Å lengthening due to the D103N mutation results in an only ~0.05 Å change in the Y16 hydrogen bond length, and the 0.13 Å lengthening of the Y16 hydrogen bond from the Y57F mutation leads to an only ~0.03 Å estimated shortening of the D103 hydrogen bond.

Conclusions and Implications. The ability to detect coupled changes in oxyanion hole hydrogen bond distances on the ~0.01 Å scale indicates that such subtle rearrangements are not swamped out by larger-scale atomic displacements within the active site from individual or collective motions of protein groups. This observation is consistent with previous studies that have suggested a tightly packed environment within the KSI active site and limited dynamic mobility of groups relative to other regions of the enzyme (*4*, *54*). Such limited mobility may enable the KSI active site to discriminate subtle geometrical changes within reacting substrates and contribute to selective transition state stabilization, as previously proposed (*4*).

While the results herein provide direct evidence for robust physical coupling of the Y16 and D103 hydrogen bond conformations on the 0.01 Å scale, the full scale of physical coupling and the attendant energetic consequences remain challenging to unravel. The D103N and Y57F mutations that perturb hydrogen bond distances within the oxyanion hole result in small (3−30-fold) reductions in k_{cat}, depending on the bacterial source of the enzyme (*25*, *27*, *28*). Furthermore, the energetic effects of the D103A and Y16F (*55*) or D103L and Y16F mutations (*56*) appear to be additive rather than cooperative, as might have been expected from substantial coupling of the two hydrogen bonds. These mutations, however, ablate one of the two oxyanion hole hydrogen bonds and result in neutral binding of phenolic transition state analogues (*25*, *57*). Thus, the connection between the physical and energetic properties of the mutant and wild-type oxyanion holes is complex.

Disentangling the physical and energetic properties of hydrogen bonds within enzyme active sites remains an ongoing challenge. The results herein provide a foundation for future experimental and computational tests and comparisons of the role of coupled motions within hydrogen bond networks.

ACKNOWLEDGMENT

We thank Corey Liu for assistance with NMR experiments and J. Brauman, H. Limbach, A. Mildvan, and P. Tolstoy for helpful discussions.

SUPPORTING INFORMATION AVAILABLE

UV absorbance spectra for $tKDI^{D103N/D40N}$·3,4,5-F_3-phenol and $tKDI^{Y57F/D40N}$·3,4,5-F_3-phenol complexes (Figure S1), a structural model of the ordered water molecule observed in the oxyanion hole of the $pKSI^{D103N/D40N}$·equilenin complex (Figure S2), and assignment of the downfield peaks observed in spectra of $tKSI^{D103N/D40N}$ and $tKSI^{Y57F/D40N}$ bound to 3,4-dinitrophenol. This material is available free of charge via the Internet at http://pubs.acs.org.

REFERENCES

(1) Jeffrey, G. A. (1997) An Introduction to Hydrogen Bonding , Oxford University Press, New York.
(2) Hibbert, F., and Emsley, J. (1990) Hydrogen bonding and chemical reactivity. *Adv. Phys. Org. Chem. 26*, 255–379.
(3) Steiner, T., and Saenger, W. (1994) Lengthening of the covalent O-H bond in O-H···O hydrogen bonds re-examined from low-temperature neutron diffraction data of organic compounds. *Acta Crystallogr. B50*, 348–357.

(4) Sigala, P. A., Kraut, D. A., Caaveiro, J. M., Pybus, B., Ruben, E. A., Ringe, D., Petsko, G. A., and Herschlag, D. (2008) Testing geometrical discrimination within an enzyme active site: Constrained hydrogen bonding in the ketosteroid isomerase oxyanion hole. *J. Am. Chem. Soc. 130*, 13696–13708.
(5) Gilli, P., Bertolasi, V., Ferretti, V., and Gilli, G. (1994) Covalent nature of the strong homonuclear hydrogen bond. Study of the O-H···O system by crystal structure correlation methods. *J. Am. Chem. Soc. 116*, 909–915.
(6) Sigala, P. A., Tsuchida, M. A., and Herschlag, D. (2009) Hydrogen bond dynamics in the active site of photoactive yellow protein. *Proc. Natl. Acad. Sci. U.S.A., 106*, 9232–9237.
(7) Fersht, A. R. (1999) Structure and Mechanism in Protein Science , 2nd ed., W. H. Freeman and Company, New York.
(8) Rodriguez, J. C., Zeng, Y. H., Wilks, A., and Rivera, M. (2007) The hydrogen-bonding network in heme oxygenase also functions as a modulator of enzyme dynamics: Chaotic motions upon disrupting the H-bond network in heme oxygenase from *Pseudomonas aeruginosa*. *J. Am. Chem. Soc. 129*, 11730–11742.
(9) Bouvignies, G., Bernado, P., Meier, S., Cho, K., Grzesiek, S., Bruschweiler, R., and Blackledge, M. (2005) Identification of slow correlated motions in proteins using residual dipolar and hydrogen-bond scalar couplings. *Proc. Natl. Acad. Sci. U.S.A. 102*, 13885–13890.
(10) Peralvarez-Marin, A., Lorenz-Fonfria, V. A., Bourdelande, J. L., Querol, E., Kandori, H., and Padros, E. (2007) Inter-helical hydrogen bonds are essential elements for intra-protein signal transduction: The role of Asp115 in bacteriorhodopsin transport function. *J. Mol. Biol. 368*, 666–676.
(11) Derege, P. J. F., Williams, S. A., and Therien, M. J. (1995) Direct evaluation of electronic coupling mediated by hydrogen-bonds: Implications for biological electron-transfer. *Science 269*, 1409–1413.
(12) Reece, S. Y., Hodgkiss, J. M., Stubbe, J., and Nocera, D. G. (2006) Proton-coupled electron transfer: The mechanistic underpinning for radical transport and catalysis in biology. *Philos. Trans. R. Soc. London, Ser. B 361*, 1351–1364.
(13) Hatcher, E., Soudackov, A. V., and Hammes-Schiffer, S. (2004) Proton-coupled electron transfer in soybean lipoxygenase. *J. Am. Chem. Soc. 126*, 5763–5775.
(14) Boehr, D. D., Dyson, H. J., and Wright, P. E. (2006) An NMR perspective on enzyme dynamics. *Chem. Rev. 106*, 3055–3079.
(15) Henzler-Wildman, K. A., Lei, M., Thai, V., Kerns, S. J., Karplus, M., and Kern, D. (2007) A hierarchy of timescales in protein dynamics is linked to enzyme catalysis. *Nature 450*, 913–916.
(16) Karplus, M., and Kuriyan, J. (2005) Molecular dynamics and protein function. *Proc. Natl. Acad. Sci. U.S.A. 102*, 6679–6685.
(17) Michalet, X., Weiss, S., and Jager, M. (2006) Single-molecule fluorescence studies of protein folding and conformational dynamics. *Chem. Rev. 106*, 1785–1813.
(18) Wales, T. E., and Engen, J. R. (2006) Hydrogen exchange mass spectrometry for the analysis of protein dynamics. *Mass Spectrom. Rev. 25*, 158–170.
(19) Agarwal, P. K., Billeter, S. R., Rajagopalan, P. T., Benkovic, S. J., and Hammes-Schiffer, S. (2002) Network of coupled promoting motions in enzyme catalysis. *Proc. Natl. Acad. Sci. U.S.A. 99*, 2794–2799.
(20) Daniel, R. M., Dunn, R. V., Finney, J. L., and Smith, J. C. (2003) The role of dynamics in enzyme activity. *Annu. Rev. Biophys. Biomol. Struct. 32*, 69–92.
(21) Pollack, R. M. (2004) Enzymatic mechanisms for catalysis of enolization: Ketosteroid isomerase. *Bioorg. Chem. 32*, 341–353.
(22) Kim, S. W., Cha, S. S., Cho, H. S., Kim, J. S., Ha, N. C., Cho, M. J., Joo, S., Kim, K. K., Choi, K. Y., and Oh, B. H. (1997) High-resolution crystal structures of Δ5−3-ketosteroid isomerase with and without a reaction intermediate analogue. *Biochemistry 36*, 14030.
(23) Wu, Z. R., Ebrahimian, S., Zawrotny, M. E., Thornburg, L. D., Perez-Alvarado, G. C., Brothers, P., Pollack, R. M., and Summers, M. F. (1997) Solution structure of 3-oxo-Δ5-steroid isomerase. *Science 276*, 415–418.
(24) Kim, D. H., Jang, D. S., Nam, G. H., Choi, G., Kim, J. S., Ha, N. C., Kim, M. S., Oh, B. H., and Choi, K. Y. (2000) Contribution of the hydrogen-bond network involving a tyrosine triad in the active site to the structure and function of a highly proficient ketosteroid isomerase from *Pseudomonas putida* biotype B. *Biochemistry 39*, 4581–4589.
(25) Kuliopulos, A., Mildvan, A. S., Shortle, D., and Talalay, P. (1989) Kinetic and ultraviolet spectroscopic studies of active-site mutants of Δ-5−3-ketosteroid isomerase. *Biochemistry 28*, 149–159.
(26) Nam, G. H., Jang, D. S., Cha, S. S., Lee, T. H., Kim, D. H., Hong, B. H., Yun, Y. S., Oh, B. H., and Choi, K. Y. (2001) Maintenance of α-helical structures by phenyl rings in the active-site tyrosine triad contributes to catalysis and stability of ketosteroid isomerase from *Pseudomonas putida* biotype B. *Biochemistry 40*, 13529–13537.
(27) Thornburg, L. D., Henot, F., Bash, D. P., Hawkinson, D. C., Bartel, S. D., and Pollack, R. M. (1998) Electrophilic assistance by Asp-99 of 3-oxo-Δ 5-steroid isomerase. *Biochemistry 37*, 10499–10506.
(28) Kim, S. W., Joo, S., Choi, G., Cho, H. S., Oh, B. H., and Choi, K. Y. (1997) Mutational analysis of the three cysteines and active-site aspartic acid 103 of ketosteroid isomerase from *Pseudomonas putida* biotype B. *J. Bacteriol. 179*, 7742.
(29) Kraut, D. A., Sigala, P. A., Pybus, B., Liu, C. W., Ringe, D., Petsko, G. A., and Herschlag, D. (2006) Testing electrostatic complementarity in enzyme catalysis: Hydrogen bonding in the ketosteroid isomerase oxyanion hole. *PLoS Biol. 4*, e99.
(30) Petrounia, I. P., and Pollack, R. M. (1998) Substituent effects on the binding of phenols to the D38N mutant of 3-oxo-Δ5-steroid isomerase. A probe for the nature of hydrogen bonding to the intermediate. *Biochemistry 37*, 700–705.
(31) Gill, S. C., and von Hippel, P. H. (1989) Calculation of protein extinction coefficients from amino acid sequence data. *Anal. Biochem. 182*, 319–326.
(32) Mccoy, A. J., Grosse-Kunstleve, R. W., Adams, P. D., Winn, M. D., Storoni, L. C., and Read, R. J. (2007) Phaser crystallographic software. *J. Appl. Crystallogr. 40*, 658–674.
(33) Murshudov, G. N., Vagin, A. A., and Dodson, E. J. (1997) Refinement of macromolecular structures by the maximum-likelihood method. *Acta Crystallogr. D53*, 240–255.
(34) Emsley, P., and Cowtan, K. (2004) Coot: Model-building tools for molecular graphics. *Acta Crystallogr. D60*, 2126–2132.
(35) Laskowski, R. A., Macarthur, M. W., Moss, D. S., and Thornton, J. M. (1993) Procheck: A program to check the stereochemical quality of protein structures. *J. Appl. Crystallogr. 26*, 283–291.
(36) Cruickshank, D. W. J. (1999) Remarks about protein structure precision. *Acta Crystallogr. D55*, 583–601.
(37) Turner, D. L. (1983) Binomial solvent suppression. *J. Magn. Reson. 54*, 146–148.
(38) Wishart, D. S., Bigam, C. G., Yao, J., Abildgaard, F., Dyson, H. J., Oldfield, E., Markley, J. L., and Sykes, B. D. (1995) ^{1}H, ^{13}C and ^{15}N chemical shift referencing in biomolecular NMR. *J. Biomol. NMR 6*, 135–140.
(39) Harris, T. K., and Mildvan, A. S. (1999) High-precision measurement of hydrogen bond lengths in proteins by nuclear magnetic resonance methods. *Proteins 35*, 275–282.
(40) Jeffrey, G. A., and Yeon, Y. (1986) The correlation between hydrogen-bond lengths and proton chemical shifts in crystals. *Acta Crystallogr. B42*, 410–413.
(41) Jencks, W. P., and Regenstein, J. (1976) Ionization Constants of Acids and Bases. In Handbooks of Biochemistry and Molecular Biology (Fasman, G. D., Ed.) pp 305−351, CRC Press, Cleveland.
(42) McDermott, A., and Rydenour, C. F. (1996) Proton Chemical Shift Measurements in Biological Solids. In Encyclopedia of Nuclear Magnetic Resonance (Grant, D. M., and Harris, R. K., Eds.) pp 3820−3824, Wiley, Hoboken, NJ.
(43) Tolstoy, P. M., Schah-Mohammedi, P., Smirnov, S. N., Golubev, N. S., Denisov, G. S., and Limbach, H. H. (2004) Characterization of fluxional hydrogen-bonded complexes of acetic acid and acetate by NMR: Geometries and isotope and solvent effects. *J. Am. Chem. Soc. 126*, 5621–5634.
(44) Steiner, T. (2002) The hydrogen bond in the solid state. *Angew. Chem., Int. Ed. 41*, 48–76.
(45) Ichikawa, M. (2000) Hydrogen-bond geometry and its isotope effect in crystals with OHO bonds—revisited. *J. Mol. Struct. 552*, 63–70.
(46) Ubbelohde, A. R., and Gallagher, K. J. (1955) Acid-base effects in hydrogen bonds in crystals. *Acta Crystallogr. 8*, 71–83.
(47) Altman, L. J., Laungani, D., Gunnarsson, G., Wennerstrom, H., and Forsen, S. (1978) Proton, deuterium, and tritium nuclear magnetic resonance of intramolecular hydrogen bonds. Isotope effects and the shape of the potential energy function. *J. Am. Chem. Soc. 100*, 8264–8266.
(48) Smirnov, S. N., Golubev, N. S., Denisov, G. S., Benedict, H., Schah-Mohammedi, P., and Limbach, H. H. (1996) Hydrogen deuterium isotope effects on the NMR chemical shifts and geometries of intermolecular low-barrier hydrogen-bonded complexes. *J. Am. Chem. Soc. 118*, 4094–4101.
(49) Jaravine, V. A., Cordier, F., and Grzesiek, S. (2004) Quantification of H/D isotope effects on protein hydrogen-bonds by h3JNC' and

1JNC' couplings and peptide group ^{15}N and $^{13}C'$ chemical shifts. *J. Biomol. NMR 29*, 309–318.
(50) Westler, W. M., Frey, P. A., Lin, J., Wemmer, D. E., Morimoto, H., Williams, P. G., and Markley, J. L. (2002) Evidence for a strong hydrogen bond in the catalytic dyad of transition-state analogue inhibitor complexes of chymotrypsin from proton-triton NMR isotope shifts. *J. Am. Chem. Soc. 124*, 4196–4197.
(51) Bolvig, S., and Hansen, P. E. (2000) Isotope effects on chemical shifts as an analytical tool in structural studies of intramolecular hydrogen bonded compounds. *Curr. Org. Chem. 4*, 19–54.
(52) Detering, C., Tolstoy, P. M., Golubev, N. S., Denisov, G. S., and Limbach, H. H. (2001) Vicinal H/D isotope effects in NMR spectra of complexes with coupled hydrogen bonds: Phosphoric acids. *Dokl. Phys. Chem. 379*, 191–193.
(53) Liu, A., Lu, Z., Wang, J., Yao, L., Li, Y., and Yan, H. (2008) NMR detection of bifurcated hydrogen bonds in large proteins. *J. Am. Chem. Soc. 130*, 2428–2429.
(54) Zhao, Q., Li, Y. K., Mildvan, A. S., and Talalay, P. (1995) Ultraviolet spectroscopic evidence for decreased motion of the active site tyrosine residue of Δ5−3-ketosteroid isomerase by steroid binding. *Biochemistry 34*, 6562.
(55) Pollack, R. M., Thornburg, L. D., Wu, Z. R., and Summers, M. F. (1999) Mechanistic insights from the three-dimensional structure of 3-oxo-Δ(5)-steroid isomerase. *Arch. Biochem. Biophys. 370*, 9–15.
(56) Jang, D. S., Cha, H. J., Cha, S. S., Hong, B. H., Ha, N. C., Lee, J. Y., Oh, B. H., Lee, H. S., and Choi, K. Y. (2004) Structural double-mutant cycle analysis of a hydrogen bond network in ketosteroid isomerase from *Pseudomonas putida* biotype B. *Biochem. J. 382*, 967–973.
(57) Petrounia, I. P., Blotny, G., and Pollack, R. M. (2000) Binding of 2-naphthols to D38E mutants of 3-oxo-Δ5-steroid isomerase: Variation of ligand ionization state with the nature of the electrophilic component. *Biochemistry 39*, 110.